NeuroImage 263 (2022) 119659

Contents lists available at ScienceDirect

NeuroImage

journal homepage: www.elsevier.com/locate/neuroimage

Structural-functional connectivity bandwidth of the human brain

Nicholas Parsons[a,*], Julien Ugon[b,‡], Kerri Morgan[b,‡], Sergiy Shelyag[b], Alex Hocking[b], Su Yuan Chan[b], Govinda Poudel[b], Juan F. Domìnguez D[a], Karen Caeyenberghs[a,c]

[a] Cognitive Neuroscience Unit, School of Psychology, Deakin University, Melbourne, VIC, Australia
[b] School of Information Technology, Faculty of Science Engineering & Built Environment, Deakin University, Melbourne, VIC, Australia
[c] Mary MacKillop Institute for Health Research, Australian Catholic University, Melbourne, VIC, Australia

A B S T R A C T

Background: The human brain is a complex network that seamlessly manifests behaviour and cognition. This network comprises neurons that directly, or indirectly mediate communication between brain regions. Here, we show how multilayer/multiplex network analysis provides a suitable framework to uncover the throughput of structural connectivity (SC) to mediate information transfer—giving rise to functional connectivity (FC).

Method: We implemented a novel method to reconcile SC and FC using diffusion and resting-state functional MRI connectivity data from 484 subjects (272 females, 212 males; age = 29.15 ± 3.47) from the Human Connectome Project. First, we counted the number of direct and indirect structural paths that mediate FC. FC nodes with indirect SC paths were then weighted according to their least restrictive SC path. We refer to this as *SC-FC Bandwidth*. We then mapped paths with the highest SC-FC Bandwidth across 7 canonical resting-state networks.

Findings: We found that most pairs of FC nodes were connected by SC paths of length two and three (SC paths of length >5 were virtually non-existent). Direct SC-FC connections accounted for only 10% of all SC-FC connections. The majority of FC nodes without a direct SC path were mediated by a proportion of two (44%) or three SC path lengths (39%). Only a small proportion of FC nodes were mediated by SC path lengths of four (5%). We found high-bandwidth direct SC-FC connections show dense intra- and sparse inter-network connectivity, with a bilateral, anteroposterior distribution. High bandwidth SC-FC triangles have a right superomedial distribution within the somatomotor network. High-bandwidth SC-FC quads have a superoposterior distribution within the default mode network.

Conclusion: Our method allows the measurement of indirect SC-FC using undirected, weighted graphs derived from multimodal MRI data in order to map the location and throughput of SC to mediate FC. An extension of this work may be to explore how SC-FC Bandwidth changes over time, relates to cognition/behavior, and if this measure reflects a marker of neurological injury or psychiatric disorders.

1. Introduction

The human brain is a complex and dynamic network comprised of both structural and functional dimensions. These dimensions can be explored with magnetic resonance imaging (MRI) to measure structural connectivity (using diffusion-weighted imaging; SC) or changes in brain activity or 'synchronicity' between brain regions (using functional connectivity; FC). Over the past decade, studies have shown a moderate correlation (~r=0.5) between these measures of brain connectivity (SC-FC) in healthy individuals (Honey et al., 2009; Honey et al., 2010; Straathof et al., 2018; Damoiseaux and Greicius, 2009; Supekar et al., 2010). More recently, there is growing interest in elucidating the complexities that drive the correlation between these types of brain connectivity. For example, statistical (Mišić and Sporns, 2016; Messé et al., 2014), communication (Goni et al., 2014; Crofts and Higham, 2009) and biophysical models (Honey et al., 2007; Breakspear, 2017) have converged to capture an imperfect correspondence between SC and FC (Suárez et al., 2020). This imperfect correspondence warrants investigation into the location and extent to which SC may mediate FC through either direct or indirect pathways (Battiston et al., 2014).

In order to consider brain connectivity at the global scale or as a "connectome", we can utilize graph theoretical analysis, enabling us to examine metrics of structural and functional graphs such as node degree (Bullmore and Bassett, 2011; Hagmann et al., 2008; Sporns, 2013) to characterize brain connectivity. An extension of graph theoretical analysis is known as a *multilayer* network analysis, allowing statistical analyses to be performed between the same nodes both within and between layers. In the context of the brain, these layers can represent different types of connectivity, such as structural or functional connectivity. We can then draw links between nodes *across layers*, termed "pseudo-edges" which can be used to represent relationships between nodes, across layers i.e., the relationship between SC and FC (SC-FC; see Fig. 1). These relationships can be modeled in the brain with a correspondence of one-to-one (i.e., multiplex; see Fig. 1), one-to-many, or many-to-many.

Multiplexes offer additional information over traditional monoplex graph theory, permitting the exploration of how functional connectivity

* Corresponding author.
E-mail address: nick.parsons@deakin.edu.au (N. Parsons).
‡ KM and JU contributed equally.

https://doi.org/10.1016/j.neuroimage.2022.119659.
Received 25 March 2022; Received in revised form 25 September 2022; Accepted 29 September 2022
Available online 1 October 2022.

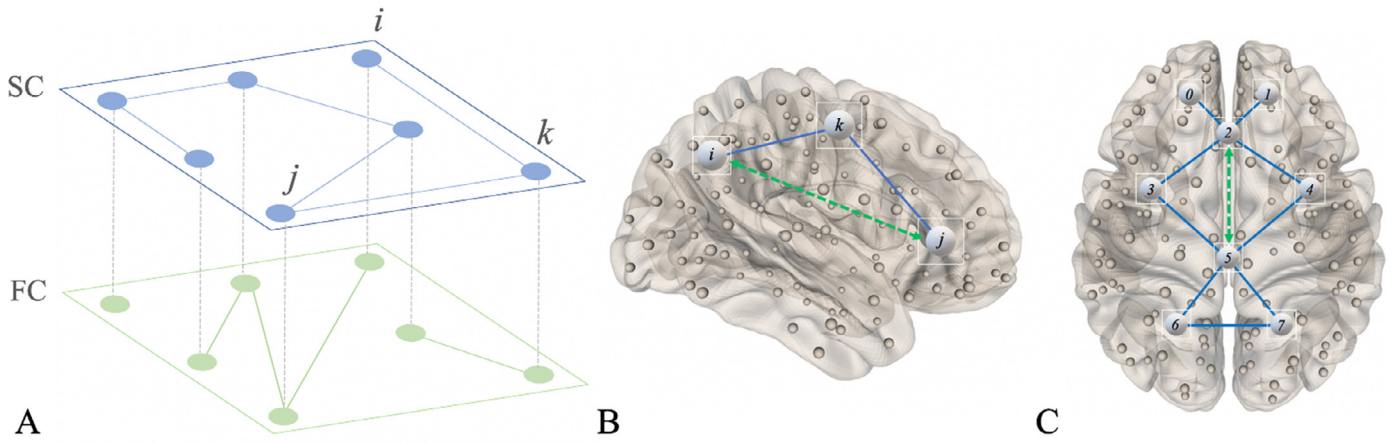

Fig. 1. A 2-layer multiplex of brain connectivity. In the brain, the upper SC layer of a multiplex represents structural connections (blue lines) between nodes (blue circles), whereas the lower FC layer represents the functional synchronicity (green lines) between these same nodes (green circles). Grey lines connecting nodes across layers represent pseudo-edges. (B) Multiplex SC-FC triangle resulting from collapsing multilayer representation. Functionally synchronous nodes i and j may functionally communicate through intermediary node k along structural edges (i,k) and (k,j). (C) Edges (2,3, 3,5) and (2,4, 4,5) form two structural tuples, each closed by an FC edge (2,5) and thus are SC-FC triangles. In contrast, edges (0,2, 2,1) and edges (5,6, 6,7) form structural tuples that are not SC-FC triangles. Therefore, the total (unweighted) number of multiplex triangles incident to the FC edge (2,5) is 2. SC edges are shown in blue and FC edges shown in green.

between nodes is mediated directly by single SC paths (i.e., edges as formally referred to in graph theory) or indirectly by multiple SC paths (multi-paths). Indeed, multiplex models have been used to quantify the proportion of overlapping high-degree SC and FC nodes (15%; Battiston et al., 2018). More recently, a predictive model estimated that direct and indirect (two-edge) SC paths may induce ~10% and up to 60% of interhemispheric FC respectively (Wang et al., 2020). Nonetheless, the proportion and location of both direct, and *indirect* SC paths that mediate FC (SC-FC polygons) across the brain remains to be explored.

SC paths are typically a secondary measure of white matter derived from diffusion MRI (dMRI), thought to comprise axons and myelin which potentiate electrical signals across the brain, permitting communication between distal brain regions (Jones, 2010). Shorter paths reduce conduction latency, synaptic retransmission and metabolic cost, which explains why on average, the shortest distance between any two nodes in an SC graph is somewhere between one and five edges (Seguin et al., 2018; Avena-Koenigsberger et al., 2019). The velocity of axon potentials that are propagated along these paths is directly proportional to both the diameter of the axon, as well as the thickness of the sheaths that insulate these axons (Rushton, 1951; Hursch, 1939). Indeed, a recent article estimated that 85% of variance in conduction velocity is accounted for by axon diameter and g-ratio (comparative thickness of the myelin sheath encasing an axon), calculated using *in-vivo* dMRI (Drakesmith et al., 2019).

SC edges comprise groups of neurons which can be considered as cables (i.e., neuronal cable theory; Cole and Hodgkin, 1939; Davis and Lorente de Nó, 1947; Hodgkin and Rushton, 1946) whereby some cables exhibit higher resistance than others, and are therefore more restrictive of information flow (i.e., throughput; Harris and Ross, 1955; Schrijver, 2002). At the macroscopic level, a recent study by Mišić, Sporns, and McIntosh (Mišić et al., 2014) applied these concepts by considering the Macaque brain as a communication network in which signal units flowed between grey matter nodes along white matter paths. Compared to a degree-matched synthetic network, they found information flow of the macaque brain showed higher loss rate, faster transit times and lower throughput, although throughput was significantly higher than a latticized control network. Upon increased load conditions, both the Macaque and synthetic networks demonstrated decreased mean transit times of signal units as a function of decreased throughput of structural pathways. Therefore, thicker, unrestricted white matter paths may have a higher capacity to propagate information (i.e., bandwidth), than thinner, restricted paths. Given SC paths can be weighted (to reflect number of streamlines or cross-section), we can measure the apparent strength of physical connections that mediate the synchronicity of brain regions (FC). For example, a low SC edge-weight may serve as a bottleneck; effectively limiting the information capacity and velocity of this path (Hursch, 1939; Rushton, 1951; Paus et al., 2014; Avena-Koenigsberger et al., 2019). In contrast, a high weight on every edge in a given path may represent a structural highway—able to communicate more information, faster.

Applications of graph metrics to describe SC-FC multiplexes, may reveal information that is beyond detection with unimodal MRI graphs. For example, studies have revealed that fMRI and EEG frequency bands show different topological properties (Domenico et al., 2016; Tewarie et al., 2016). Others have reported lower assortativity of FC (-0.15), and higher assortativity of SC (0.1) which may indicate a robustness to acute injury or neurodegeneration (Lim et al., 2019). Importantly, these methods hinge on either the comparison of two distinctly different measurements (i.e., SC and FC) or the co-dependency (correlation) of nodes or layers as a whole, without offering insight into the location and extent to which SC mediates the efficient propagation of information from one node to another.

Work by Crofts et al. (2016) recognised the difference between the structural and functional layers in their multiplex adaptation of the clustering coefficient, using simulated, directed FC of the Macaque brain. This method considers triangles comprised of two SC edges connected by an intermediary centroidal structural node (i.e., structural tuple) closed by an FC edge. SC-FC triangles pertaining to centroidal nodes can then be quantified as a multiplex nodewise "clustering coefficient" (Crofts et al., 2016). This local clustering coefficient measures the proportion of structural tuples that are closed by an FC edge (forming a multiplex polygon, in this case a multiplex triangle), out of the total number of SC tuples that exist (see Fig. 1 for examples of SC tuples and SC-FC triangles). This measure is able to elucidate areas of parameter space in which "clustering" is dominated by *indirect* functional connectivity. However, this measure only reflects the number of binary SC-FC triangles that SC nodes are incident to.

According to our knowledge, there has been no study that has examined the number of paths that mediate synchronicity between brain regions, or their weights. Moreover, no consideration has been given to the possibility that there may be functionally synchronous nodes that communicate through multiple indirect structural paths, comprising mul-

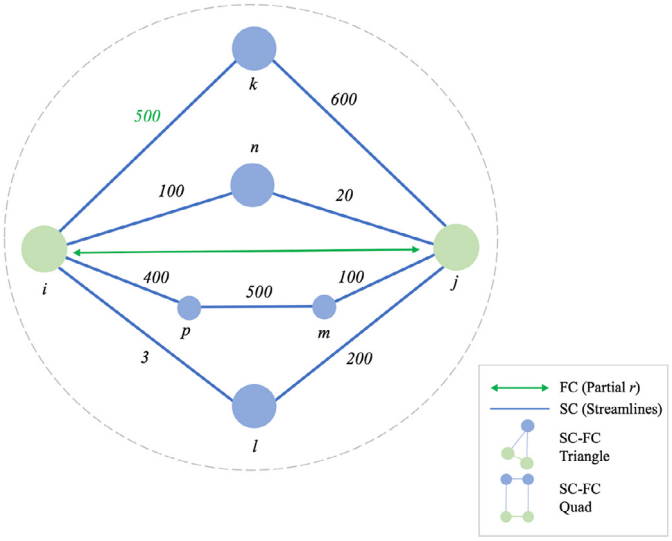

Fig. 2. A schematic showing two functionally synchronous nodes (i and j) connected by multiple structural tuples ((i,k), (k,j)), ((i,n), (n,j)), ((i,l), (l,j)) and one quad ((i,p), (p,m), (m,j)). Our method weights SC-FC polygons by their largest minimum edge weight (in blue) between functionally synchronous nodes i and j (in green). The maximum bandwidth of nodes (i and j) irrespective of polygon type is thus 500 streamlines, through the tuple (i.e., SC-FC triangle) using the path i-k-j, as this value is higher than the largest minimum edge weight of any other path. As a reference point, the bandwidth of the quad ((i,p), (p,m), (m,j)) is 100.

tiple structural connectivity weights (Fig. 2). This forms the basis for which we consider what a structural layer can tell us about a functional edge. To investigate this requires a conceptual shift away from considering the number of triangles that a single SC node is incident to (as per Crofts et al., 2016) and toward considering information about the structural paths that mediate indirect communication between a pair of functionally synchronous nodes. Moving forward, we propose a graph theoretic methodology leveraging the concept that structural connections provide the physical infrastructure that "*constrains, maintains and regulates*" functional communication (Straathof et al., 2018, p39). Subsequently, we introduce a graph metric utilizing an SC-FC multiplex to quantify the bandwidth of functional synchronous nodes throughout the human brain that are mediated by direct and indirect SC, which we term "SC-FC Bandwidth".

Our aims are fourfold:

(i) To implement a novel technique to measure the proportion of functionally synchronous brain regions that are mediated by direct and indirect structural pathways.
(ii) To examine the relationship between our novel graph metric and existing measures.
(iii) To quantify the bandwidth of SC-FC polygons that mediate FC.
(iv) To map the spatial distribution of SC-FC bandwidth across the human brain.

2. Method

2.1. Primary Sample

In the present study, we utilized a publicly available dataset, provided by the Human Connectome Project (HCP; http://www.humanconnectome.org) from the Washington University-University of Minnesota (WUMinn) consortium, including 484 healthy participants from the Q4 release (500 subject; Nov 25, 2014; 272 females, 212 males; age = 29.15 ± 3.47). For details on the MRI pre-processing and connectivity matrix calculation, the interested reader is referred to Lim et al. (2019).

2.2. Secondary Sample (MICA)

In addition to our primary dataset, we conducted a secondary control analysis, using SC (measured as number of reconstructed streamlines) and FC (measures as Pearson's correlation coefficient) connectomes from an open-source independent data set of 50 healthy adults (23 women; 29.54 ± 5.62 years) as part of the Multimodal MRI dataset for Microstructure-Informed Connectomics (MICA; Royer et al., 2022). These connectomes were parsed in the Schaefer atlas (Schaefer et al., 2018) with a resolution of 200 nodes for maximum comparability with our primary dataset. The MICA dataset has already been described extensively within Royer et al., (2022). Hereafter, we will briefly describe pre- and post-processing steps of our primary dataset (HCP).

2.3. MRI Data Acquisition (HCP)

Data were acquired using a modified 3T Siemens Skyra scanner with a 32-channel head coil. Resting-state fMRI data in an eyes-open condition were collected for approximately 14 min (1,200 volumes) with TR = 720ms, TE = 33.1ms, flip angle = 52, voxel size = 2mm isotropic, FOV = 208 × 180mm^2 and 72 slices with opposite phase encoding directions in two runs (L-R, R-L). In addition, T1- weighted structural images (MPRAGE) were acquired using the following parameters: TR = 2,400ms, TE = 2.14ms, flip angle = 8 degrees, voxel size = 0.7mm isotropic, FOV = 224 × 224mm^2 and 320 slices. Diffusion-weighted images (DWI) were acquired with 270 gradient directions (90 per shell; multi-shell) with *b*-values 1000, 2000, 3000mm^2, with 90 gradient encoding directions in each shell TR = 5520ms, TE = 89.5ms, flip angle = 78, FOV = 210 × 180mm^2, 111 slices, and voxel size = 1.25mm isotropic.

2.4. Diffusion and Functional MRI Pre-processing

From the minimally pre-processed HCP diffusion-weighted MRI data, white matter fibres were reconstructed using generalized q-sampling imaging (Yeh et al., 2010) and deterministic streamline tractography was performed (Yeh et al., 2013) using DSI studio (http://dsi-studio.labsolver.org). The HCP minimally processed fMRI data were first realigned and co-registered to T1-weighted structural images using FSL (Jenkinson et al., 2012). Motion in the form of linear trends and/or first order drifts with global effects were regressed out of white matter, ventricular, and global mean signals, using 6 motion parameters in Matlab R2016b (MATLAB 2018). White matter and ventricle voxels were then segmented using T1-weighted images in FreeSurfer (Fischl, 2012). Time-series were then band-pass filtered (0.01–0.1 Hz). Motion scrubbing was used to remove scan frames when significant motion was detected in the individual time series. Diffusion and functional MRI scans from each subject used in this study were extracted from the HCP 500 Q4 data release and minimally preprocessed by the HCP consortium; further details on the specific steps employed can be found in Glasser et al. (2013). The pre-processed fMRI time-series of each region of interest was subsequently used to compute partial correlation coefficients between each region of interest, as outlined in the section "Construction and Thresholding of SC and FC Adjacency Matrices", below.

2.5. Parcellation

We utilised a multi-resolution atlas derived from the Desikan-Killiany cortical atlas excluding sub-cortical areas in line with (Cammoun et al., 2012). Here, each parcel from the original 68 resolution is subdivided twice to produce three resolutions of the same atlas. Analyses were repeated at all three parcellation resolutions (68,

114, 219) to ensure that effects were independent of matrix resolution as recommended by several studies (Mansour et al., 2021; Vàzquez-Rodríguez et al., 2019; Zalesky et al., 2010). We decided to focus on the positive correlations only, as the current understanding of negative correlations/negative edge weights in whole-brain connectivity is limited (Zhan et al., 2017); see discussion section. Our method utilises a one-to-one mapping between nodes on each layer (i.e., matched parcellation/node density), which has implications for increasing FC and SC node density. That is, increasing FC node density comes at the cost of reducing correlation values (and subsequently thresholding-out FC edges), resulting in a sparser, weaker graph, with reduced ability to model SC-FC polygons across the brain. Similarly, SC node density must be high enough to accurately model pathways. Therefore, we report our findings using 219 nodes for both SC and FC graphs hereafter. We organized these nodes according to seven canonical resting-state network including the visual network, somatomotor network, dorsal attention network, ventral attention network, limbic network, frontoparietal network and default mode network (Yeo et al., 2011).

2.6. Construction and Thresholding of SC and FC Adjacency Matrices

FC adjacency matrices from each subject comprised partial correlation coefficients, which have been shown to reduce spurious correlation effects (Smith et al., 2013). These adjacency matrices were thresholded using regularization based on an elastic-net regression model to overcome specific limitations of regularisation penalties. L1-norm regularization only detects a subset of highly correlated connections and L2-norm regularisation does not threshold-out (convert to a value of 0) small correlation coefficients; which may compromise the trade-off between sparseness and the removal of spurious correlations (Zou and Hastie, 2005). Elastic-net regression uses both L1- and L2-norm regularization, or a linear combination of the two, depending on the coefficient (Friedman et al., 2008; Lim et al., 2019). For example, a coefficient of 1 is subject to the L1-norm model (resulting in a sparser graph). Therefore, this model overcomes limitations of partial correlations albeit at the cost of lower FC values (Krämer et al., 2009; Ryali et al., 2012; Nie et al., 2015; Friedman et al., 2008; Lim et al., 2019) and sparser graphs, relative to bivariate pairwise correlation coefficients (Sanchez-Romero and Cole, 2020). Neurobiologically speaking, it has been argued that the brain is highly integrative and therefore, connections represented by low partial correlation values should arguably be considered as weak—that is, the connections represented by these values are indistinguishable from noise (Bielczyka et al., 2018). These noisy connections can influence the sparsity of FC networks, in turn altering the structural properties of the connectome (van den Heuvel et al., 2017; Zalesky et al., 2016). Therefore, we supplemented the regularization of partial correlation values by applying an empirical precision with a hard thresholding approach. Specifically, this involves setting a fixed value of partial correlation (0.1), at which empirical connectomes are thresholded (Bielczyka et al., 2018).

SC adjacency matrix edge weights were defined as the number of reconstructed streamlines between two ROI derived from diffusion MRI deterministic tractography (see Lim et al., 2019). This measurement reflects the number of tracts connecting two brain regions, and was chosen for maximum comparability with existing diffusion MRI studies (Jeurissen et al., 2019). At the individual level, SC, FC and weighted SC-FC (see Weighted SC-FC Triangle Throughput) were constructed for each individual subject, resulting in 484 FC, 484 SC (thresholded to exclude number of streamline values lower than one) and 484 weighted SC-FC connectomes which were used for subsequent analyses. At the group level, a group-average weighted SC-FC matrix was then computed using the sum of all matrix values across individuals divided by 484. All post-processing of adjacency matrices was completed using (MATLAB 2018) (http://www.mathworks.com) and Python (version 3.0). Our full weighted and unweighted multiplex connectivity python code can be found here: https://github.com/parsonsn/SC-FC-Multiplex-Bandwidth. Full mathematical details of our method are provided in supplementary material.

2.7. Unweighted SC Pathways Closed by an FC Edge

Brain network communication may rely on direct structural connections (a single edge), tuples (two edges) or paths with three or more edges. Here, we establish the contribution of each pathway type to mediate FC. For every FC edge, we count the minimum number of associated structural edges. Firstly, we count the number of single (direct) SC edges (Fig. 3). We count only FC edges that have corresponding SC edges to avoid over-representing single-edge SC connections. Secondly, we count SC paths of edge length two (i.e., tuple; see Fig. 2). And finally, we count SC paths of edge length larger than two (See Fig. 2). In addition, we used the "Proportion of SC-FC Polygons" Formula below, to compute the expected proportion of shortest path length in Erdős-Rényi randomized graphs with the same density as our SC graphs for each subject to compare standard deviations across individuals, and to contrast our empirical values with what would be expected if the graphs were random. The Erdős-Rényi model is a good predictor of diameter and average path length compared to real networks, resulting in networks with small diameters, capturing the "small-world" property observed in human brain networks. Specifically, the expected proportion of the shortest paths of length k in an Erdős-Rényi graph with n vertices and density d is:

$$\left(1-\left(1-d^{k}\right)^{\frac{(n-2)}{(n-1-k)}}\right)\prod_{j=1}^{k-1}\left(1-d^{j}\right)^{\frac{(n-2)}{(n-1-j)}}$$

2.8. Weighted SC-FC Bandwidth Calculation

Here, we introduce mathematical notations for weighted measurements.

- $A^{[\alpha]}$ is the adjacency matrix for Layer α, where α is s (for structural layer) or f (for functional layer);
- $A_{ij}^{[\alpha]}$ is the entry at position (i,j) in the adjacency matrix for Layer α;
- $w_{ij}^{[\alpha]}$ is the weight of edge (i,j) on Layer α.

We quantify the bandwidth between two synchronous regions according to their minimum edge weight ("max-min method"; see Fig. 2). These paths may support higher signal capacity and velocity (Hursch, 1939; Rushton, 1951; Paus et al., 2014; Avena-Koenigsberger et al., 2019) relative to other paths incident to a given FC edge (for the mathematical representation of this measure, see Equation 2). That is, the SC throughput of an SC-FC polygon (direct = 1 SC edge; triangle = 2 SC edges; quad = 3 SC edges) is equal to its largest and thus least restrictive bottleneck. Effectively, this measurement reflects the *communication bandwidth* of each FC edge. Higher bandwidth values incident to a given FC edge therefore reflect throughput of synchronous nodes.

The weighted throughput of each SC-FC triangle is:

$$T_{ij}= A_{ij}^{[f]}\left(1-A_{ij}^{[s]}\right)\max_{k\in V}\left(\min\left(w_{ik}^{[s]},w_{kj}^{[s]}\right)\right)$$

where V is the set of nodes. Any triangle containing a functional edge (i,j) and structural edges (i,k) and (k,j) has a structural edge of minimum weight. In line with our analogy of the structural layer being akin to a communication network, this minimum weight provides the maximum possible throughput from i to j in this tuple on the structural layer. We consider each vertex k in our set of nodes V, i.e., $k \in V$, as a possible intermediary node. Finally, we are only interested in tuples that are triangles containing a functional edge (i,j) which we count using $A_{ij}^{[f]}$ and excluding cases where there is also a structural edge (i,j) which are excluded using the $(1-A_{ij}^{[s]})$ term.

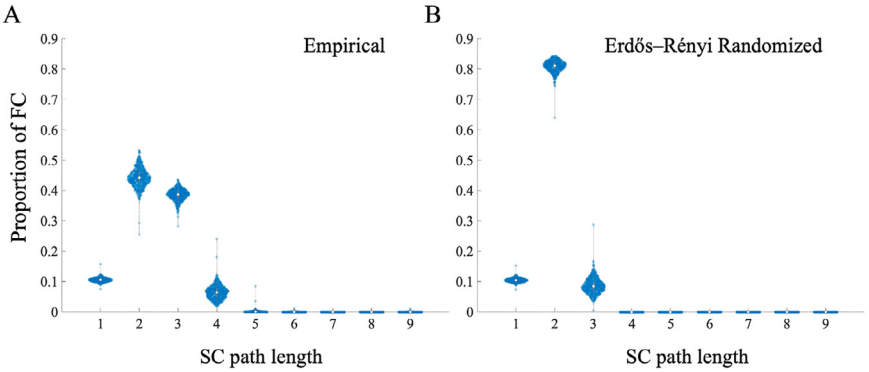

Fig. 3. Violin plots showing the proportions of FC edges that are closed by a range of path lengths (from 1-9 edges) for all 484 subjects. Panel A shows the number of SC paths connecting FC edges when using empirical data, and Panel B shows the number of SC paths connecting FC edges when using Erdős-Rényi randomized graphs as SC and FC inputs for each subject. Points are drawn as outliers if they are larger than Q3+W*(Q3-Q1) or smaller than Q1-W*(Q3-Q1), where W = whisker length, and Q1 and Q3 are the 25th and 75th percentiles, respectively.

2.9. Weighted, Direct SC-FC Equation

$$D_{ij} = A_{ij}^{[s]} A_{ij}^{[f]} w_{ij}^{[s]}$$

2.10. Weighted SC-FC Quad Equation

The *weight* of a path ik_1k_2j is calculated as $\min(w_{ik_1}^{[s]}, w_{k_1k_2}^{[s]}, w_{k_2j}^{[s]})$. Given two vertices i and j, we consider the path with the largest of the minimum of these weights ($\max_{k_1,k_2 \in V} \min(w_{ik_1}^{[s]}, w_{k_1k_2}^{[s]}, w_{k_2j}^{[s]})$) as the highest throughput pathway. The weighted throughput of each SC-FC quad is:

$$Q_{ij} = A_{ij}^{[f]}\left(1 - \hat{D}_{ij} - \hat{T}_{ij}\right) \max_{k_1,k_2 \in V} \left(\min\left(w_{ik_1}^{[s]}, w_{k_1k_2}^{[s]}, w_{k_2j}^{[s]}\right)\right)$$

Note: $\hat{D}_{ij} = \begin{cases} 0 & \text{if } D_{ij} = 0 \\ 1 & \text{otherwise} \end{cases}$

Note: $\hat{T}_{ij} = \begin{cases} 0 & \text{if } T_{ij} = 0 \\ 1 & \text{otherwise} \end{cases}$

2.11. Weighted SC-FC Bandwidth Equation for Path Length $n+1$

$$w_{ij}^{[b](n)} = A_{ij}^{[f]}\left(1 - \sum_{p=0}^{n-1} A_{ij}^{[b](p)}\right) \max_{k_1,k_2,\ldots,k_n \in V} \left(\min\left(w_{ik_1}^{[s]}, w_{k_1k_2}^{[s]}, \ldots, w_{k_nj}^{[s]}\right)\right) w_{ij}^{[b](1)} = A_{ij}^{[f]} A_{ij}^{[s]} w_{ij}^{[s]}$$

2.12. Proportion of SC-FC Polygons

For each FC edge ij, we calculate the shortest SC path connecting vertices i and j. The proportion of SC-FC polygons gives the proportion of FC edges that have shortest SC paths of length l, given as

$$FC_{prop}(l) = \frac{\sum_{ij \in F} P_{ij}(l)}{|F|}$$

where F is the set of FC edges and $P_{ij}(l) = \begin{cases} 1 & \text{if the shortest SC path connecting } ij \text{ has length } l \\ 0 & \text{otherwise.} \end{cases}$

3. Results

3.1. Proportion of Direct and Indirect Structural Paths Mediating Functional Connectivity

Across subjects, we found most FC nodes were indirectly connected, and relatively few were directly connected. Empirical FC nodes were most frequently connected by two SC edges (i.e., tuple; 44%) followed by three-path (triplet) SC edges (39%) and direct (one-path) SC edges (10%; see Fig. 3). We did not investigate beyond path length of nine as the small-worldness of brain networks suggests paths of this length are unlikely to exist (Bullmore and Bassett, 2011; Avena-Koenigsberger et al., 2019). As such, we found the shortest possible path between *most* functionally synchronous nodes was two (i.e., SC-FC triangles), and the largest number of paths was four. When compared with the expected proportions of shortest paths of length k (for $k = 1 \ldots, 9$) in Erdős-Rényi randomized graphs, we found a similar proportion of direct SC-FC pathways ($k = 1$) with empirical data (~10%) and different proportions of FC paths facilitated by SC paths of length two and three. The proportion of paths of length of five and higher was negligible using both empirical and randomized data (<.001).

3.2. Relationships Between FC, SC-FC Bandwidth and Euclidean Distance

To explore SC-FC Bandwidth in the context of known measurements, we conducted several statistical analyses. Herein, we plotted SC-FC Bandwidth values with partial correlation coefficient and Euclidean distance of each edge. First, we observed a linear trend when comparing partial correlation coefficient and SC-FC Bandwidth. Therefore, we chose to model these data using a linear Pearson's correlation coefficient. Secondly, we observed nonlinear trends in scatterplots of Euclidean distance and SC-FC Bandwidth data across polygon types, as well as in three-dimensional plots of Euclidean distance, partial correlation coefficient and SC-FC Bandwidth. Therefore, we chose to model these data with polynomial fit models, to capture any nonlinear relationships (see Fig. 4 and Online Supplementary Figure 1). Results revealed a divergent pattern below and above bandwidth values of 10 streamlines across all polygon types: for SC-FC Bandwidth values below 10, we found no relationship between FC or Euclidean distance. For SC-FC Bandwidth values above 10, we found a strong positive linear correlation between group-average FC (partial correlation coefficients) and bandwidth in direct paths (r=0.71, p=<0.001; Fig. 4). In other words, the greater the SC-FC Bandwidth, the higher the FC. Regarding SC-FC triangles and quads, the relationship between FC and SC-FC Bandwidth was also positive, but substantially weaker (r=0.18, p=<0.001, and r=0.17, p =<0.001, respectively; Fig. 4). We found the Euclidean distance between FC nodes decays exponentially in relation to SC-FC Bandwidth (direct; adjusted R^2=0.32, triangle; adjusted R^2=0.26, quad; adjusted R^2=0.11; Fig. 6B); thus, SC-FC Bandwidth slope increases with Euclidean distance up to bandwidth of 100, and very slowly past this point. The slope of this increase is progressively less with a greater number of SC paths, as evident in the shallower curves in triangles and quads. The plot for direct paths (Fig. 4C) suggests that the greater the SC-FC Bandwidth and Euclidean distance, the higher the FC (adjusted R^2=0.63). For SC-FC triangles (adjusted R^2=0.11) and quads (adjusted R^2=0.05) this triadic relationship is less pronounced as reflected by lower adjusted R^2 squared values. Collectively, these findings indicate that high-bandwidth edges

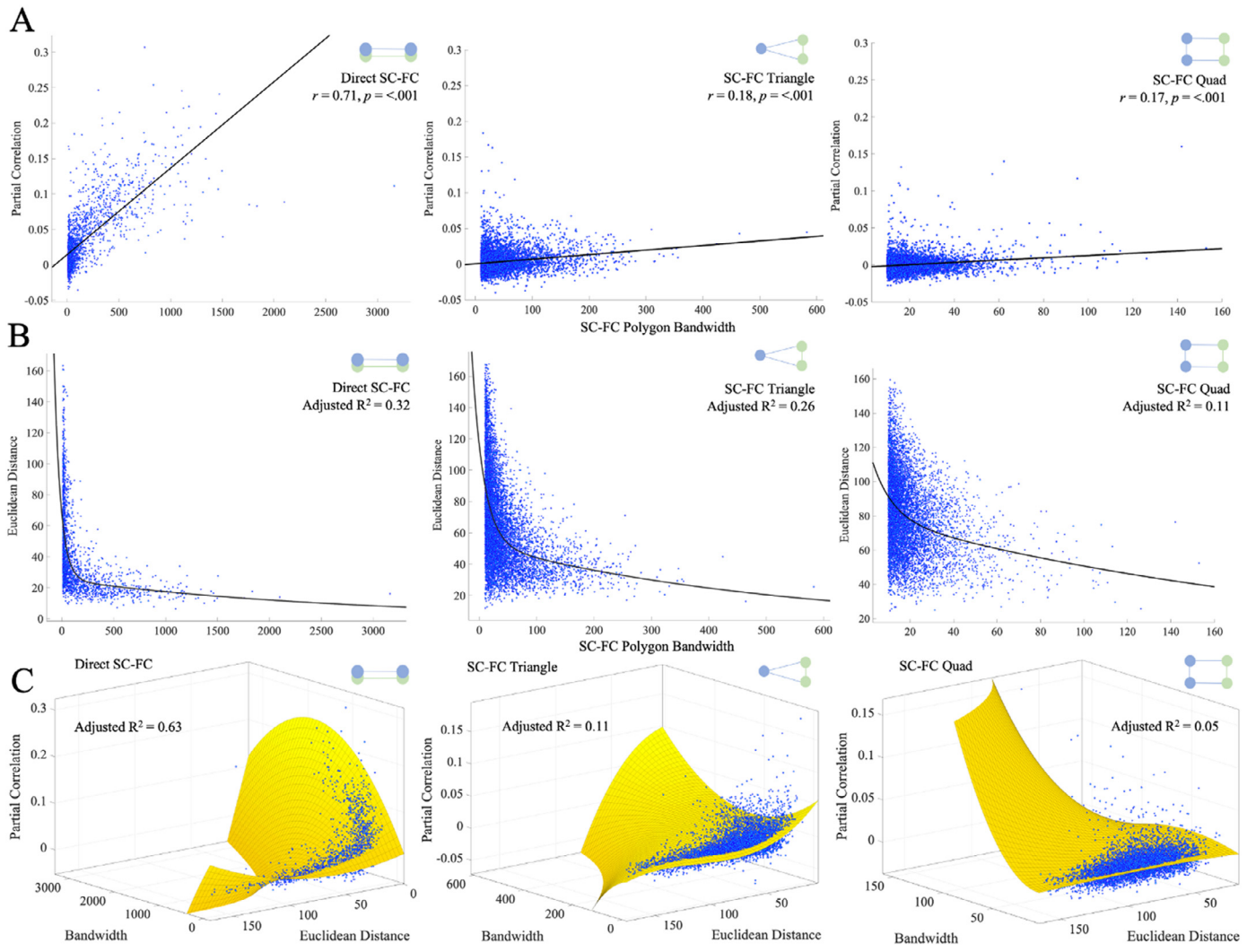

Fig. 4. SC-FC bandwidth in the context of known measurements. (A) Scatterplots and linear correlations between group-average SC-FC polygon bandwidth and group-average partial correlation coefficient of each FC edge for direct SC-FC (left), SC-FC triangles (middle), and SC-FC quads (right). (B) Scatterplots and negative exponential fit models between group-average SC-FC polygon bandwidth and group-average Euclidean distance of each FC edge of direct SC-FC (left), SC-FC triangles (middle), and SC-FC quads (right). (C) Three-dimensional plots showing triadic relationships between SC-FC polygon bandwidth, group-average partial correlation coefficient and Euclidean length of each FC edge for direct SC-FC (left), SC-FC triangles (middle), and SC-FC quads (right).

have particular biological significance—warranting further exploration into the spatial distribution of these high-bandwidth edges across the brain.

3.3. Spatial Distribution of High-Bandwidth SC-FC Polygons

As shown in the section "Proportion of Direct and Indirect Structural Paths Mediating Functional Connectivity", the relationship between FC, SC-FC Bandwidth and Euclidean distance highlighted the significance of high-bandwidth polygons. Therefore, we examine the distribution of high SC-FC Bandwidth edges hereafter. Specifically, we focus on the highest 200 SC-FC Bandwidth (4th percentile) edges, to balance specificity (i.e., clear visualization of spatial patterns) and sensitivity (i.e., more robust SC-FC Bandwidth edges; Zalesky et al., 2016). High-bandwidth *direct* SC-FC connections show a bilateral, anteroposterior distribution (Fig. 5A, B; Top) and highest bandwidth between right superiorfrontal and left superiorfrontal nodes. SC-FC triangles have a right superomedial distribution, with the highest *indirect* bandwidth between right precentral and paracentral nodes, and between left precentral and postcentral nodes within the somatomotor network (Fig. 5C; middle). High-bandwidth SC-FC quads have a superoposterior distribution (Fig. 5A, B; Bottom) and regions with the highest indirect SC-FC bandwidth include left inferior parietal, right inferior parietal, right precuneus and inferior parietal nodes within the default mode network (Fig. 5C; Bottom). Maximum SC-FC Bandwidth diminishes with SC path length (i.e., direct, triangle, quads, respectively; Fig. 5A,B,C). Intra-network connectivity was highest in direct SC-FC (Supplementary Fig. 7C; median = 15), followed by SC-FC triangles (Supplementary Fig. 7C; median = 4) and SC-FC quads (Supplementary Fig. 7C; median = 2). Inter-network connectivity was highest in SC-FC triangles (Supplementary Fig. 7B; median = 30) compared to quads (Supplementary Fig. 7C; median = 28) and direct SC-FC (Supplementary Fig. 7A; median = 13). Inter-network connectivity was lowest in direct SC-FC (Supplementary Fig. 7C; median = 13). Finally, we found that median bandwidth is highest in direct SC-FC (48.33), followed by SC-FC triangles (25.24) and quads (15.64) suggesting SC-FC polygons with less SC paths have the highest bandwidth.

3.4. Inter-subject Variability of Mean SC-FC Bandwidth

Due to the high frequency of SC-FC triangles identified in our results, we focus on these SC-FC polygons to examine the inter-subject

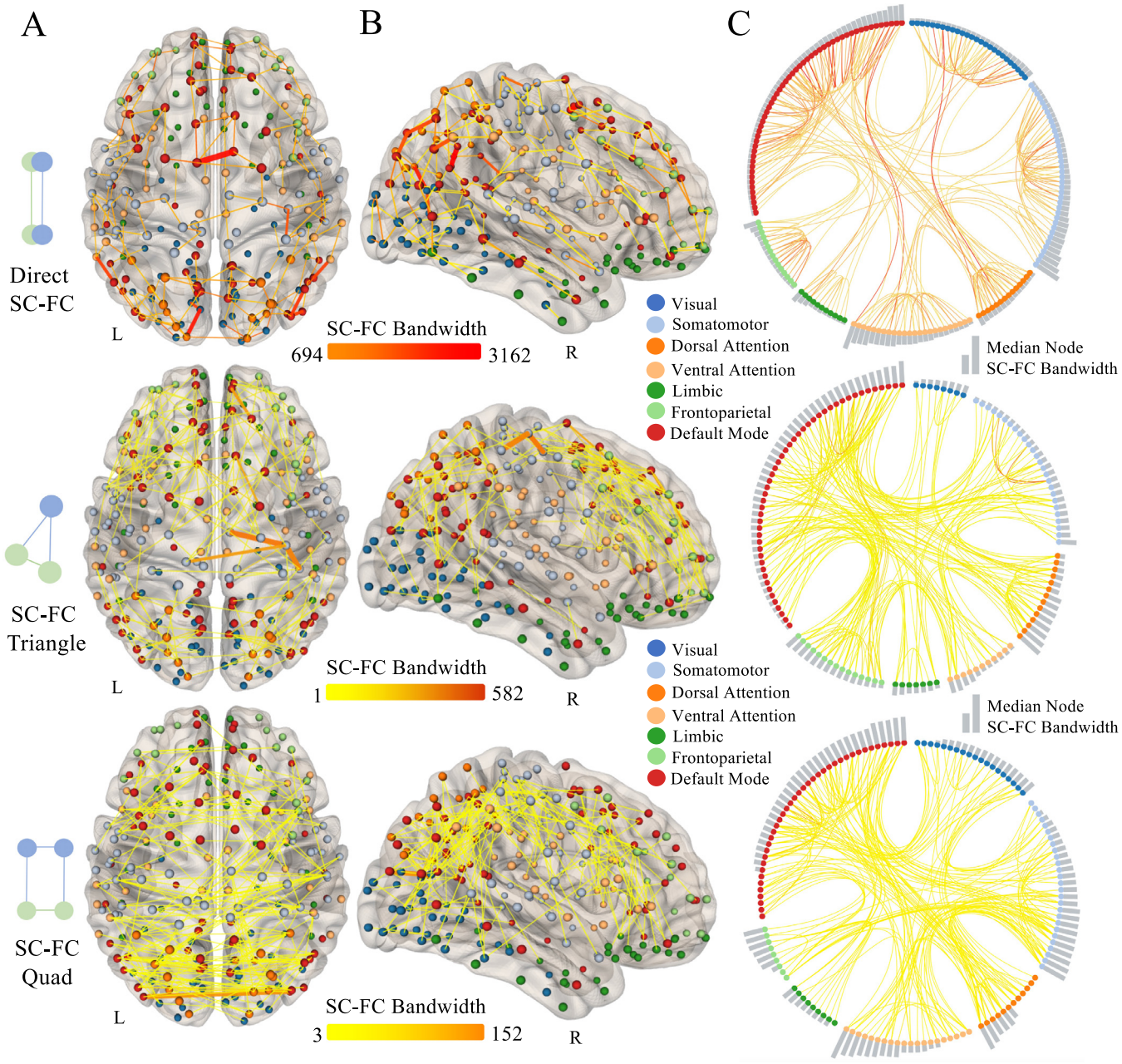

Fig. 5. Spatial distribution of high SC-FC bandwidth edges. Top: (A) Axial and (B) Sagittal spatial distribution of high group average weighted SC-FC Bandwidth of direct SC-FC (Top), SC-FC triangles (middle) and SC-FC quads (Bottom) at 219 resolution (see Equation 1). (C) Connectome rings showing high group average SC-FC Bandwidth within and between 7 canonical resting-state networks (Yeo et al., 2011) and median SC-FC bandwidth incident to each node. Highest 200 edges weights shown; where edge thickness is proportional to edge weight.

variability of mean SC-FC Bandwidth values in the context of an independent data set (MICA) and parcellation scheme (Schaefer atlas) as a control analysis. As shown above, violin plots of mean SC-FC Bandwidth values show relatively consistent distributions across parcellation schemes, within 7 canonical resting-state networks, using both HCP data parsed with the Desikan-Killiany atlas, and MICA data parsed with the Schaefer atlas using similar resolutions (219 and 200 nodes, respectively). One-way analysis of variance (ANOVA) revealed these mean SC-FC Bandwidth are significantly different across canonical resting-state network using both the HCP data parsed with the Desikan-Killiany atlas ($F(6,484) = 227$, $p<.001$) and MICA data parsed with the Schaefer atlas ($F(6,50)=13.77$, $p<.001$).

4. Discussion

With this paper, we propose a paradigm-shift toward considering how and where structural connections may constrain, maintain and regulate communication between brain regions. Leveraging a multiplex framework, we measured the number of paths, bandwidth and spatial distribution of direct and indirect SC polygons to mediate FC edges. Subsequently, we introduce a novel graph theoretical measurement termed—*SC-FC Bandwidth*. Using our method, we uncover the capacity of white matter microstructure to mediate FC in the human brain. These findings contribute to the emerging characterization of the structural-functional connectivity relationship. Hereafter, we discuss

our main findings with respect to our three aims, raise key methodological considerations, identify study limitations and provide suggestions.

To address our first aim, we measured the proportion of functionally synchronous brain regions that are facilitated by direct and indirect structural pathways. Our results revealed that few functionally synchronous brain regions are facilitated by direct SC edges, and most are facilitated indirectly by SC tuples (SC-FC triangles). These findings lend support to Wang et al. (2020) who predicted SC from FC by applying a model with a prediction rate above 60% when including indirect (length-two) paths; suggesting a large number of FC nodes may be facilitated by indirect SC. Although the proportion of single (direct) paths could be replicated using randomized graphs, we could not replicate proportions of tuples and triplets (paths of length three) using randomized data for each subject—suggesting ubiquitous indirect connectivity in the human brain has biological significance.

The disparity between random and empirical data can be explained by a number of factors. First, our Erdős-Rényi graphs were density-matched (i.e., the same number of edges as our empirical data). That is, the expected diameter (the largest number of vertices which must be traversed in order to travel from one vertex to another, or longest shortest paths) is small. Therefore, a similar proportion of paths of length one was expected. Regarding the proportion of longer paths, our formula shows that the proportion of paths of length k decreases quickly beyond $k = 3$ in random graphs of this type. Regarding paths of length two and three, the proportion of these is randomized (within the constraints imposed; i.e., density) and therefore is not expected to coincide with the proportion of these paths found in empirical data.

We found no overlap between high-bandwidth indirect SC-FC and known hub-hub SC of the default mode network (Alves et al., 2019), suggesting direct and indirect connectivity may work in unison to support FC. In addition, our finding of ubiquitous indirect connectivity (SC-FC triangles) lends credibility to the notion that the human brain has well-known "small world" properties for a reason; i.e. a balance between integration and segregation in order to be robust to single node failure while also maintaining cost-efficient transmission of information (Bassett and Bullmore, 2006; Bullmore and Sporns, 2009; van den Heuvel and Sporns, 2011). Furthermore, due to the inconsistent topological organisation of the brain (left and right hemispheric subnetworks), direct paths (i.e., a single large white matter fibre bundle such as the corpus callosum) can facilitate communication between some, but not all contralateral and/or distal nodes. It is conceivable that these direct paths may also obstruct other nodes, where few crossing fibres exist. In some instances, additional anatomical structures may further obstruct these nodes (e.g., lateral ventricles). In these instances, SC-FC triangles and quads represent the next best available option to propagate information from one distal/contralateral node to another. The high frequency of SC-FC triangles is therefore unsurprising, as these SC-FC polygons comprise relatively few paths, to facilitate relatively disconnected brain regions.

To address our second aim, we found that direct SC-FC polygons tend to have higher bandwidth, and higher corresponding partial correlation coefficients which may reflect higher cost-efficiency (i.e., lower metabolic cost) relative to SC-FC triangles and quads. The significance of direct high-bandwidth SC-FC polygons is yet to be explored, although studies have linked efficiency and cost-efficiency with executive task performance using fMRI (van den Heuvel et al., 2009), MEG (Bassett et al., 2009), and diffusion MRI (Li et al., 2009). The spatial distribution of high-bandwidth SC-FC polygons can be considered within the context of recent efforts to map the distribution of SC-FC Pearson's correlation values across the brain using a multilinear regression model (Vàzquez-Rodríguez et al., 2019). Indeed, this model uncovered higher node-specific SC-FC R^2 values of unimodal cortices such as the primary sensory and motor regions, and lower node-specific SC-FC R^2 values in trans-modal cortices within the default mode and salience networks, where these nodes do not explain a high amount of variance in SC-FC correlation values. Extending upon this work, we report that default mode network nodes exhibit high information capacity relative to nodes in other networks which cannot be modelled using (a) traditional linear modelling assumptions, and (b) consideration of only direct SC paths (Vàzquez-Rodríguez et al., 2019). Here, our findings contribute to the emerging *nonlinear* characteristics of SC-FC relationships in human brain networks. Our work also extends upon recent applications of SC-FC multiplex analyses such as (Lim et al., 2019) who reported network-specific assortativity of SC-FC correlation values geared toward the dorsal attention and frontoparietal networks. Importantly, both Vàzquez-Rodríguez et al. (2019) and Lim et al. (2019) utilize measures of dependency (i.e., correlation coefficient) which although useful at describing general relationships between two variables, cannot describe how information transfer between FC nodes is mediated by SC. Therefore, our method and subsequent novel graph metric represents an important transition toward explaining how the structure-function relationship is facilitated, by considering the capacity of individual nodes to propagate information—ultimately giving rise to functional communication.

To address our third aim, we implemented a novel mathematical model within a multiplex framework to quantify the bandwidth of SC-FC polygons. Higher bandwidth values incident to a given FC edge reflect greater throughput of synchronous nodes. Our method extends upon (Crofts et al., 2016) who quantified binary centroidal node participation within SC-FC triangles, to instead consider weighted structural paths that link functionally synchronous brain regions within common SC-FC polygon types (i.e., direct, triangles and quads). Subsequently, our measure offers information above and beyond SC-FC triangle participation.

To address our fourth aim, we mapped the spatial distribution of nodes with high SC-FC bandwidth across the brain. We report that high bandwidth SC-FC triangles and quads pertain to the somatomotor and default mode networks, respectively. At a nodal level, we found the highest indirect bandwidth (SC-FC triangles) between right precentral gyral nodes. These nodes are connected by the corticospinal tract, where sensory information can be relayed to and from the peripheral nervous system. The internal pyramidal layer (V) of the precentral cortex contains large (70-100 micrometres) pyramidal neurons (Betz cells) which project long axons to the contralateral motor nuclei of the cranial nerves, and to the lower motor neurons in the ventral horn of the spinal cord. These axons form the bilateral corticospinal tract. Therefore, proximal precentral cortex nodes are indirectly linked, by different portions of a large white matter fibre bundle (the corticospinal tract) which may explain their synchronicity (due to their proximity) and high (indirect) bandwidth.

We found high bandwidth SC-FC quads predominate the default mode network. This network is generally thought to be mediated by white matter pathways including the anterior and posterior cingulum, the uncinate, superior longitudinal, arcuate, and inferior longitudinal fasciculi and frontal orbito-polar tracts (Tiepel et al., 2010; Buckner et al., 2008). However, a broader extension of this network has recently been proposed to include several sub-cortical gray matter regions (thalamus and basal forebrain; Alves et al., 2019), highlighting the potential to model sub-cortical modulation of large-scale networks within multiplex analyses. Therefore, a natural extension of our work may include mapping which intermediary white matter fibre tracts mediate FC between the precuneus and inferior parietal cortex, and how the distribution/bandwidth of SC-FC polygons may be affected by sub-cortical white matter fibre bundle projections. At a nodal level, we found the highest bandwidth exists between inferior parietal and precuneus nodes. This discovery is fitting, given the known hypermetabolism of the posterior cingulate cortex (~40% higher than average; Raichle et al., 2001; Pfefferbaum et al., 2010) relative to other brain areas. A combination of higher metabolism and higher SC-FC Bandwidth may reflect the highly heterogeneous role of the PCC within the default mode, right frontparietal control, dorsal attention, salience, sensorimotor and left frontoparietal control networks (Leech and Sharp, 2010).

Our novel graph metric quantifies the bandwidth of two synchronous nodes (i.e., brain regions) according to their largest minimum edge

weight which we term the "max-min method". This method is akin to a circuit- or message-switched architecture (Graham and Rockmore, 2011) where all data are sent along one path. However, this method ignores alternate, more restrictive paths between these same nodes. For example, our measure does not sum the total bandwidth of multiple polygons with lower throughput (i.e., sum of multiple max-min paths). To sum multiple high-bandwidth paths would be akin to a packet-switched architecture, in which a signal may be broken into smaller "packets" of signal(s) which take the most efficient path to the target node where they are then re-assembled (Graham and Rockmore, 2011). These assumptions have important implications regarding the role that alternate paths may play in enabling the propagation of electrical information from one region to another. Hereafter, we discuss each of these architectural assumptions in greater detail.

In our case, the decision not to sum alternate paths within our SC-FC Bandwidth equation is based on several considerations. Firstly (a) we rely upon references supporting that the larger the axon, the higher the throughput (Harris and Ross, 1955; Schrijver, 2002). From these references, our max-min theory follows using mathematical principles. However, we do not have evidence to suggest that we can sum all polygons that facilitate two functionally synchronous nodes (either linearly, or polynomially or otherwise). For example, it could be that bandwidth grows quadratically with the number of streamlines, and it is not true that $(a + b)^2 = a^2 + b^2$. Therefore, the values that we obtain cannot be added without additional assumptions which may not hold. On the other hand, calculating the max-min only requires the assumption that less bandwidth means fewer streamlines.

Secondly, (b) our SC-FC Bandwidth equation assumption (akin to a circuit-switched architecture) fits within a growing body of research suggesting human neural networks are already organized for optimal communication efficiency (Avena-Koenigsberger et al., 2019; Seguin et al., 2018). For example, it is known that the number of axons is directly proportional to gray matter volume across 59 mammalian species (Laughlin and Sejnowski, 2003) and the folds of the human cerebral cortex minimize the total lengths of axons required to join them (Klyachko and Stevens, 2003; Simoncelli and Olshausen, 2001). Shorter axons increase conduction velocity and decrease voltage entropy (Hodgkin and Rushton, 1946; Spruston et al., 2013; Beierlein, 2014), making these paths more efficient than longer paths. The axons comprising these paths are organized to balance integration and segregation (i.e., small worldness; Bassett and Bullmore, 2017; Watts and Strogatz, 1998) whilst also reducing signal traffic (Laughlin and Sejnowski, 2003) and wiring cost (Cherniak, 1992; Mitchison, 1991). Following these insights, it is reasonable to posit that wiring cost and signal traffic would be optimized by using singular, high-bandwidth paths where such paths exist, as opposed to splitting information into packets between several paths in order to facilitate ongoing functional communication between source and target nodes. This is because the fundamental principle underpinning axonal conduction velocity (Hursch, 1939; Rushton, 1951) states that the speed of signal is necessarily affected by the thickness of axons, as well as the sheaths that insulate these axons. Therefore, paths with differential bandwidth necessarily transmit signals as differential velocity. In other words, signals that are split into packets must reach target nodes at different times which could make seamless communication between source and target nodes difficult.

4.1. Computational Results in the Context of Histological Work

Firstly, our finding of high inter-hemispheric SC-FC Bandwidth particularly of direct SC-FC polygons) is intuitive, given 99% of interhemispheric corticocortical axons are routed through the corpus callosum (CC; Aboitiz et al., 1992; Highley et al., 1999; Rosen and Halgren, 2022) and therefore, all inter-hemispheric SC-FC polygons necessarily make use of the CC. Secondly, our finding that SC-FC Bandwidth decreases exponentially with longer SC-FC polygons, and longer Euclidean distance is consistent with the exponential decline of SC with Euclidean distance reported elsewhere (Markov et al., 2013). However, our finding of higher direct SC-FC Bandwidth relative to SC-FC triangles and quads is intrinsic to our Max-min model, where longer paths (i.e., paths with more "hops") increase the likelihood of a low SC edge (i.e., low weighted sub-path), and thus a lower overall bandwidth. In other words, the more hops between nodes, the more chance of encountering a low-weighted (i.e., restrictive) edge, restricting the SC-FC Bandwidth of the entire path.

Our finding of low empirical SC-FC quad frequency is consistent with histological studies reporting long-range corticocortical fibres are relatively sparse, precluding a direct connection between most contralateral brain regions (Rosen and Halgren, 2022) which is partly mitigated by small-world network architecture (Watts and Strogatz, 1998; Bassett and Bullmore, 2017). These long-range white matter connections are thought to arise due to the tendency of axons to develop or adhere in alignment with existing axons toward a common distal target—termed fasciculation (Spead and Poulain, 2020). By virtue of this process, it is commonly assumed that axons span the entire length of these tracts via a structural "highway", though an alternate theory suggests these axons terminate at various points along white matter tracts (trans-terminal) which may explain why crossing fibres can be identified in up to 90% of voxels (Jeurissen et al., 2013). To inform this theory, Rosen and Halgren (Rosen and Halgren, 2022) estimated packing density (Zikopoulos and Barbas, 2010) and tract diameter (Yeh, 2020) of the arcuate and superior longitudinal fasciculus terminating at Broca's and Wernicke's areas. They reported only a fraction of these ipsilateral axons were trans-terminal (1-5%) supporting the "highway" theory. However, since the corpus callosum does not project to any specific cortex, and each fibre bundle likely comprises different histological features (i.e., mean axonal diameter, size of termination field, axonal arborization, molecular synaptic specialization; Deco et al., 2021), these findings may not be generalizable beyond the arcuate and superior longitudinal fasciculi. Moving forward, there is opportunity to reconcile macroscopic and histological features of common indirect SC pathways that utilize the CC, or other large white matter fibre bundles.

4.2. Methodological Considerations

Importantly, the edges in our group average SC layer represent the number of reconstructed streamlines using deterministic tractography, yet it is unclear whether this is the most appropriate measurement of SC, despite being arguably the most popular (Jeurissen et al., 2019). The number of reconstructed streamlines essentially represents a stream or track from a starting location (seed) in a direction using the local fibre orientation guided by individual voxels (deterministic; one streamline per voxel). Alternatively, probabilistic tractography simulating multiple streamlines samples per seed voxel drawn from the local fibre orientation distribution (Jones, 2010; Calamante, 2019; Dhollander et al., 2020) should be used in future work to evaluate our findings. Further, a fundamental limitation of this technology is its non-quantitative nature, i.e., the density of reconstructed connections is not reflective of the density of underlying white matter fibres (Smith et al., 2015). As such, deterministic tractography is prone to false negatives, and is inherently a second-order white matter measurement which does not necessarily reflect information pertaining to the white matter microstructure (i.e., axon diameter). For instance, specific diffusion MRI measures relating to axon and myelin such as axon density, axon diameter, and myelin water fraction may provide richer insight underlying SC (Ganzetti et al., 2014; Glasser and Essen, 2011). More recently, total intra-axonal cross-sectional area of a fibre bundle (or Fibre Bundle Capacity; FBC) has emerged as measure that can be used as proxy for the "bandwidth" of a connection, i.e., the capacity of a fibre bundle to transfer information (Smith et al., 2020). Each of these measures may contribute unique information about microstructural properties, albeit with trade-offs relating to each (Uddin et al., 2019). Therefore, there is ample room to

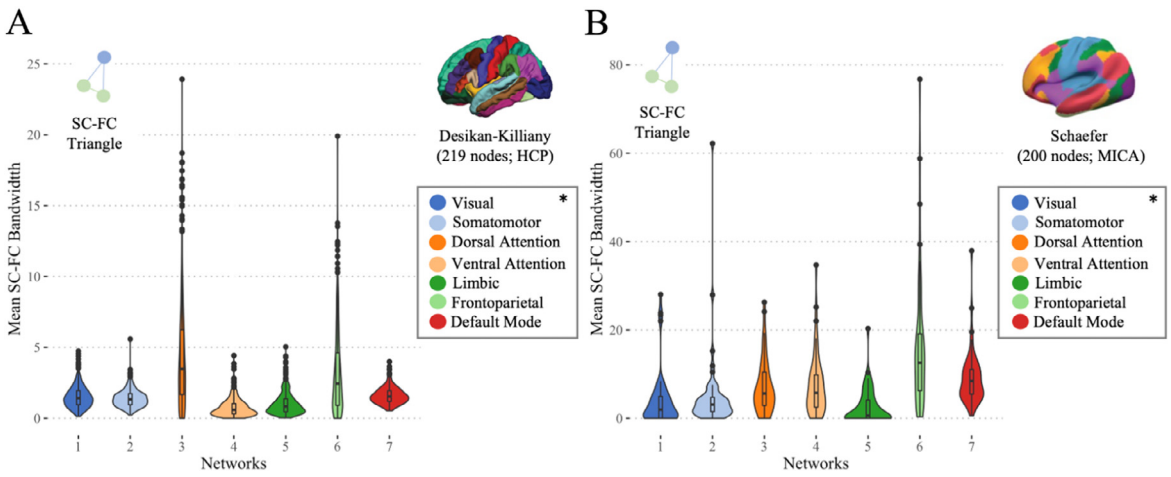

Fig. 6. Inter-subject variability of mean SC-FC bandwidth across canonical resting-state networks and parcellation schemes. Panel A shows violin plots of mean SC-FC bandwidth values (SC-FC triangles) for each HCP subject, across 7 canonical resting-state networks using the Desikan-Killiany atlas with 219 node resolution. Panel B shows violin plots of mean SC-FC bandwidth values (SC-FC triangles) for each MICA subject, across 7 canonical resting-state networks using the Schaefer atlas with 200 node resolution. *Colors correspond with violin plots.

consider how alternative SC measures relate to FC within a multiplex framework.

SC-FC bandwidth depends on the position, size and density of FC nodes, as well as the number and location of SC paths that connect these nodes. Therefore, the spatial distribution of high-bandwidth edges cannot be resolution or atlas invariant. This issue pertains to any graph metric, for which to the best of our knowledge, there remains no solution. This issue highlights the need to justify the choice of multiplex parcellation scheme. Moving forward, we propose the use of one-to-many multiplex mapping; where the connectivity between pairs of FC nodes from a coarse-grained atlas (for example Desikan Killaney 68 cortical resolution) is modeled using ultra high-resolution SC (i.e., ~1:1000 edges, respectively). Though we report and interpret group-level SC-FC Bandwidth, variation exists within each subject with respect to mean values (as shown in Figure 6) as well as the anatomic location of these values. Therefore, we present our interpretation of group-level findings as an example of how our method can be applied. Moving forward, there is opportunity to link global or local SC-FC maps from each subject with cognition, to determine the value of SC-FC bandwidth toward predicting specific cognitive processes that may be linked to information capacity (e.g., processing speed).

Important to note, our findings do not completely explain the biological mechanism underpinning information transfer between nodes. Rather, our novel graph metric is an *apparent* higher-order model to characterize information transfer capacity between nodes. In future, studies may wish to enrich higher-order multiplexes with simulated temporal waveforms (Hansen et al., 2015), excitatory/inhibitory fMRI spike-firing models (Schirner et al., 2018; Breakspear, 2017), and resting-state neural dynamics (Mišić and Sporns, 2016). Due consideration must also be given to if and how to include negative correlations within SC-FC multiplex models which forms the basis for why we excluded these values from our analyses. Although it is generally established that the dorsal attention network is anti-synchronous with the default mode network (Dixon et al., 2017; Fox et al., 2005; Fransson, 2005; Golland et al., 2008) and that the salience network acts as intermediary between these two networks (Seeley, 2019; Seeley et al., 2007), the meaning of these negative (anti) correlations in neuroscience is still unclear. However, given the nature of an aggregated resting-state FC layer, one might consider exploring how negative correlations derived from dynamic or task-based FC are facilitated by SC-FC polygons. Lastly, we found no relationship between SC-FC Bandwidth values below 10 and Euclidean distance or partial correlation coefficient in any polygon type–suggesting that these edges may not have biological significance or may represent noise.

5. Conclusion

The introduction of this novel graph metric paves the way to explore how the bandwidth of synchronous brain regions relate to cognition, disease or acute injury. In brain-injured patients, a reduced structure-function relationship highlights the potential for multiplex analyses to shed light on how and where injury to focal grey- or white-matter affects SC-FC polygons, and if these polygons demonstrate alterations in response to injury (Parsons et al., 2020). In addition to understanding how and where SC mediates FC between nodes, there is growing interest in predicting FC matrices using SC matrices within machine learning approaches. For example, some have predicted FC with accuracy that exceeds biophysical models whilst explaining inter-individual variation in cognitive performance (Sarwar et al., 2021). Although these techniques can predict FC with moderate accuracy, machine-learning cannot yet explain how the complex interplay of biophysical variables manifests an individual's FC signature. As such, a reconciliation between machine-learning approaches and multiplex analyses represents a powerful and enigmatic prospect.

Funding

Nicholas Parsons is supported by a Deakin University Postgraduate Research Scholarship (DUPRS). Julien Ugon is supported by ARC Discovery Project DP180100602. Karen Caeyenberghs grant IDs APP1143816 is supported by a National Health and Medical Research Council Career Development Fellowship. Alex Hocking is funded by an internal funding scheme within the Faculty of Science, Engineering and Built Environment, Deakin University.

Ethics statement

Participants were recruited by the WU-Minn HCP consortium and provided written informed consent prior to experiments. All experimental procedures were approved by the Institutional Review Board (IRB) at Washington University and no further IRB approval was required for our data analysis.

Data and code availability statement

Our full source code can be found at: https://github.com/parsonsn/SC-FC-Multiplex-Bandwidth. In the present study, we utilized a publicly available dataset, provided by the Human Connectome Project (HCP; http://www.humanconnectome.org) from the Washington University-University of Minnesota (WU- Minn) consortium, including 484 healthy participants from the Q4 release (500 subject; Nov 25, 2014).

Declaration of Competing Interest

The authors do not have any conflicts of interest to declare.

Credit authorship contribution statement

Nicholas Parsons: Conceptualization, Data curation, Methodology, Formal analysis, Project administration, Validation, Visualization, Writing – original draft, Writing – review & editing. **Julien Ugon:** Conceptualization, Methodology, Writing – review & editing. **Kerri Morgan:** Conceptualization, Methodology, Writing – review & editing. **Sergiy Shelyag:** Conceptualization, Methodology, Validation. **Alex Hocking:** Formal analysis, Software, Validation. **Su Yuan Chan:** Writing – review & editing. **Govinda Poudel:** Supervision, Writing – original draft, Writing – review & editing. **Juan F. Domìnguez D:** Conceptualization, Formal analysis, Methodology, Writing – original draft, Writing – review & editing. **Karen Caeyenberghs:** Conceptualization, Supervision, Writing – original draft, Writing – review & editing.

Data availability

Data will be made available on request.

Acknowledgments

Data were provided (in part) by the Human Connectome Project, WU-Minn Consortium (Principal Investigators: David Van Essen and Kamil Ugurbil; 1U54MH091657) funded by the 16 NIH Institutes and Centres that support the NIH Blueprint for Neuroscience Research; and by the McDonnell Centre for Systems Neuroscience at Washington University.

Supplementary materials

Supplementary material associated with this article can be found, in the online version, at doi:10.1016/j.neuroimage.2022.119659.

References

Aboitiz, F, Scheibel, A B, Fisher, R S, Zaidel, E, 1992. Fiber composition of the human corpus callosum. Brain Res. 598 (1-2), 143–153.
Alves, P.N., Foulon, C., Karolis, V., Bzdok, D., Margulies, D.S., Volle, E., de Schotten, M.T., 2019. An improved neuroanatomical model of the default-mode network reconciles previous neuroimaging and neuropathological findings. Commun. Biol. 2 (370).
Avena-Koenigsberger, A., Yan, X., Kolchinsky, A., van den Heuvel, M.P., Hagmann, P., Sporns, O., 2019. A spectrum of routing strategies for brain networks. PLoS Comput. Biol. 24 pages.
Bassett, D.S., Bullmore, E.T, 2006. Small-world brain networks. Neuroscientist 12 (6), 512.
Bassett, D.S., Bullmore, E., Meyer-Lindenberg, A., Weinberger, D.R., Coppola, R., 2009. Cognitive fitness of cost- efficient brain functional networks. Proc. Natl. Acad. Sci. United States America 106, 11747–11752.
Bassett, Danielle S, Bullmore, Edward T, 2017. Small-world brain networks revisited. Neuroscientist 23 (5), 499–516.
Battiston, F., Guillon, J., Chavez, M., Latora, V., De Vico Fallani, F., 2018. Multiplex core–periphery organization of the human connectome. J. R. Soc., Interface 15 (146), 20180514.
Battiston, F., Nicosia, V., Latora, V., 2014. Structural measures for multiplex networks. Phys. Rev. E 89 (3).
Beierlein, Michael., 2014. Cable properties and information processing in dendrites. In: From Molecules to Networks. Elsevier, pp. 509–529. doi:10.1016/b978-0-12-397179-1.00017-8.
Bielczyka, N., Walochaa ans P. W. Ebela, F., Haaka, K.V., Lleraa, A., Buitelaara, J.K., Glennona, J.C., Beckmann, C.F., 2018. Thresholding functional connectomes by means of mixture modeling. Neuroimage 171, 402–414.
Breakspear, Michael., 2017. Dynamic models of large-scale brain activity. Nat. Neurosci. 20 (3), 340–352.
Buckner, R.L., Andrews-Hanna, J.R., Schacter, D.L., 2008. The brain's default network: anatomy, function, and relevance to disease. Year Cognit. Neurosci. 1124, 1–38.
Bullmore, E.T., Bassett, D.S., 2011. Brain graphs: graphical models of the human brain connectome. Annu. Rev. Clin. Psychol. 7, 113–140.
Bullmore, E., Sporns, O., 2009. Complex brain networks: graph theoretical analysis of structural and functional systems. Nat. Rev. Neurosci. 10, 186–198.
Calamante, F., 2019. The seven deadly sins of measuring brain structural connectivity using diffusion MRI streamlines fibre-tracking. Diagnostics (Basel) 9 (3), 115.
Cammoun, L., Gigandeta, X., Meskaldjia, D., Thirana, J.P., Spornsb, O., Doc, K.Q., Maederd, P., Meulid, R., Hagmann, P., 2012. Mapping the human connectome at multiple scales with diffusion spectrum MRI. J. Neurosci. Methods 203, 386–397.
Cherniak, Christopher., 1992. Local optimization of neuron arbors. Biol. Cybern. 66 (6), 503–510. doi:10.1007/bf00204115.
Cole, K.S., Hodgkin, A.L., 1939. Membrane and protoplasm resistance in the squid giant axon. J. Gen. Physiol. 22, 671–687.
Crofts, J.J., Forrester, M., O'Dea, R.D., 2016. Structure-function clustering in mulitplex brain networks. Europhys. Lett. 116 (1), 18003.
Crofts, Jonathan J, Higham, Desmond J, 2009. A weighted communicability measure applied to complex brain networks. J. R. Soc., Interface 6 (33), 411–414.
Damoiseaux, J., Greicius, M., 2009. Greater than the sum of its parts: a review of studies combining structural connectivity and resting-state functional connectivity. Brain Struct. Funct. 213 (6), 525–533.
Davis Jr, L.D., Lorente de Nó, R, 1947. Stud. Rockefeller Inst. Med. Res. 131, 422.
Deco, Gustavo, Sanz Perl, Yonathan, Vuust, Peter, Tagliazucchi, Enzo, Kennedy, Henry, Kringelbach, Morten L, 2021. Rare long-range cortical connections enhance human information processing. Curr. Biol. 31 (20), 4436–4448 e5.
Dhollander, T., A. Clemente, M. Singh, F. Boonstra, O. Civier, J. F. Domínguez, N. Engrova, et al. 2020. "Fixel-based analysis of diffusion MRI: methods, applications, challenges and opportunities."
Dixon, M.L., Andrews-Hanna, J.R., Spreng, R.N., Irving, Z.C., Mills, C., Girn, M., Christoff, K., 2017. Interactions between the default network and dorsal attention network vary across default subsystems, time, and cognitive states. Neuroimage 147, 632–649.
Domenico, M.De, Sasai, S., Arenas1, A., 2016. Mapping multiplex hubs in human functional brain networks. Front Neurosci 10, 326.
Drakesmith, Mark, Harms, Robbert, Rudrapatna, Suryanarayana Umesh, Parker, Greg D., John Evans, C., Jones, Derek K., 2019. Estimating axon conduction velocity in vivo from microstructural MRI. Neuroimage 203, 116186. doi:10.1016/j.neuroimage.2019.116186.
Fischl, B., 2012. Freesurfer. Neuroimage 62, 774–781.
Fox, M., Snyder, A.Z., Vincent, J.L., Corbetta, M., Van Essen, D.C, Raichle, M.E., 2005. The human brain is intrinsically organized into dynamic, anticorrelated functional networks. Proc. Natl. Acad. Sci. United States America 107 (27), 9673–9678.
Fransson, P., 2005. Spontaneous low-frequency BOLD signal fluctuations: an fMRI investigation of the resting-state default mode of brain function hypothesis. Hum. Brain Mapp. 26 (1), 15–29.
Friedman, J., Hastie, T., Tibshirani, R., 2008. Sparse inverse covariance estimation with the graphical lasso. Biostatistics 9, 432–441.
Ganzetti, M., Wenderoth, N., Mantini, D., 2014. Whole brain myelin mapping using T1- and T2-weighted MR imaging data. Front. Hum. Neurosci. 8, 671.
Glasser, M.F., Sotiropoulos, S.N., Wilson, J.A., Coalson, T.S., Fischl, B., Andersson, J.L., Xu, J., et al., 2013. WU-Minn HCP consortium. The minimal preprocessing pipelines for the human connectome project. Neuroimage 80, 105–124.
Glasser, M., Van Essen, D.C., 2011. Mapping human cortical areas in vivo based on myelin content as revealed by T1- and T2-weighted MRI. J. Neurosci. 31 (32), 11597–11616.
Golland, Y., Golland, P., Bentin, S., Malach, R., 2008. Data-driven clustering reveals a fundamental subdivision of the human cortex into two global systems. Neuropsychologia 46 (2), 540–553.
Goni, J., van den Heuvel, M.P., Avena-Koenigsberger, A., Velez de Mendizabal, N., Betzel, R.F., Griffa, A., Hagmann, P., Corominas-Murtra, B., Thiran, J.-P., Sporns, O., 2014. Resting-brain functional connectivity predicted by analytic measures of network communication. Proc. Natl. Acad. Sci. 111 (2), 833–838.
Graham, Daniel, Rockmore, Daniel, 2011. The packet switching brain. J. Cogn. Neurosci. 23 (2), 267–276. doi:10.1162/jocn.2010.21477.
Hagmann, P., Cammoun, L., Gigandet, X., Meuli, R., Honey, C.J., Van Wedeen, J., Sporns, O., 2008. Mapping the structural core of human cerebral cortex. PLoS Biol. 6 (7), 1–15.
Hansen, Enrique C.A., Battaglia, Demian, Spiegler, Andreas, Deco, Gustavo, Jirsa, Viktor K., 2015. Functional connectivity dynamics: modeling the switching behavior of the resting state. Neuroimage 105, 525–535 January.
Harris, T.E., Ross, F.S., 1955. Fundamentals of a Method for Evaluating Rail Net Capacities. US Airforce Project Research Memorandum RM-1573.
Heuvel, M.P.van den, de Lange, S.C., Zalesky, A., Seguin, C., Yeo, B.T.T., Schmidt, R., 2017. Proportional thresholding in resting-state fMRI functional connectivity networks and consequences for patient-control connectome studies: issues and recommendations. Neuroimage 152, 437–449.
Heuvel, M.P.van den, Stam, C.J., Kahn, R.S., Hulshoff Pol, H.E, 2009. Efficiency of functional brain networks and intellectual performance. J. Neurosci. 29, 7619–7624.
Heuvel, M.van den, Sporns, O., 2011. Rich-club organization of the human connectome. J. Neurosci. 31 (44), 15775–15786.
Highley, J R, Esiri, M M, McDonald, B, Roberts, H C, Walker, M A, Crow, T J, 1999. The size and fiber composition of the anterior commissure with respect to gender and schizophrenia. Biol. Psychiatry 45 (9), 1120–1127.

Hodgkin, A.L., Rushton, W.A.H., 1946. The electrical constants of a crustacean nerve fibre. Proc. R. Soc. London. Ser. B - Biol. Sci. 133 (873), 444–479.
Honey, C.J., Kotter, R., Breakspear, M., Sporns, O., 2007. Network structure of cerebral cortex shapes functional connectivity on multiple time scales. Proc. Natl. Acad. Sci. 104 (24), 10240–10245.
Honey, C.J., Thivierge, J-P, Sporns, O., 2010. Can structure predict function in the human brain? Neuroimage 52, 766–776.
Honey, C., Sporns, O., Cammoun, L., Gigandet, X., Thiran, J., Meuli, R., Hagmann, P., 2009. Predicting human resting-state functional connectivity from structural connectivity. Proc. Natl. Acad. Sci. 106 (6), 2035–2040.
Hursch, J.B., 1939. Conduction velocity and diametre of nerve fibre. Am. J. Physiol. 127, 131–139.
Jenkinson, M., Beckmann, C.F., Behrens, T.E., Woolrich, M.W., Smith, S.M., 2012. Fsl. Neuroimage 62, 782–790.
Jeurissen, B., Descoteaux, M., Mori, S., Leemans, A., 2019. Diffusion MRI fiber tractography of the brain. NMR Biomed. 34 (2).
Jeurissen, Ben, Leemans, Alexander, Tournier, Jacques-Donald, Jones, Derek K, Sijbers, Jan, 2013. Investigating the prevalence of complex fiber configurations in white matter tissue with diffusion magnetic resonance imaging. Hum. Brain Mapp. 34 (11), 2747–2766.
Jones, D., 2010. Challenges and limitations of quantifying brain connectivity in vivo with diffusion MRI. Imaging Med. 2 (3), 341–355.
Klyachko, Vitaly A., Stevens, Charles F., 2003. Connectivity optimization and the positioning of cortical areas. Proc. Natl. Acad. Sci. 100 (13), 7937–7941. doi:10.1073/pnas.0932745100.
Krämer, N., Schäfer, J., Boulesteix, A.L., 2009. Regularized estimation of large-scale gene association networks using graphical Gaussian models. BMC Bioinf. 10, 384.
Laughlin, Simon B., Sejnowski, Terrence J., 2003. Communication in neuronal networks. Science 301 (5641), 1870–1874. doi:10.1126/science.1089662.
Leech, R., Sharp, D., 2010. The role of the posterior cingulate cortex in cognition and disease. Brain 137, 12–32.
Li, Y., Liu, Y., Qin, W., Li, K., 2009. Brain anatomical networks and intelligence. PLoS Comput. Biol. 5, e1000395.
Lim, S., Radicchi, F., van den Heuvel, M., Sporns, O., 2019. Discordant attributes of structural and functional brain connectivity in a two-layer multiplex network. Sci. Rep. 9 (1).
Mansour, S., Tian, Ye, Yeo, Thomas, Cropley, Vanessa, Zalesky, Andrew, 2021. High-resolution connectomic fingerprints: mapping neural identity and behavior. Neuroimage 229 (1), 117695.
Markov, Nikola T, Ercsey-Ravasz, Mária, Essen, David C Van, Knoblauch, Kenneth, Toroczkai, Zoltán, Kennedy, Henry, 2013. Cortical high-density counterstream architectures. Science 342 (6158), 1238406.
MATLAB, 2018. Version 9.4 (R2018a). The MathWorks Inc, Natick, Massachusetts.
Messé, Arnaud, Rudrauf, David, Benali, Habib, Marrelec, Guillaume, 2014. Relating structure and function in the human brain: relative contributions of anatomy, stationary dynamics, and non-stationarities. Edited by Claus C. Hilgetag. PLoS Comput. Biol. 10 (3), e1003530.
Mišić, Bratislav, Sporns, Olaf, 2016. From regions to connections and networks: new bridges between brain and behavior. Curr. Opin. Neurobiol. 40, 1–7 October.
Mišić, Bratislav, Sporns, Olaf, McIntosh, Anthony R., 2014. Communication efficiency and congestion of signal traffic in large-scale brain networks. Edited by Danielle S. Bassett. PLoS Comput. Biol. 10 (1), e1003427.
Mitchison, Graeme. 1991. "Neuronal branching patterns and the economy of cortical wiring." *Proc. R. Soc. Lond. B Biol. Sci.* 245 (1313): 151–58. doi:10.1098/rspb.1991.0102.
Nie, L., Yang, X., Matthews, P.M., Xu, Z., Guo, Y., 2015. Minimum partial correlation: an accurate and parameter-free measure of functional connectivity in fMRI. Lecture Notes in Computer Science Vol. 9250. Springer, CHAM.
Parsons, N., M. E. Hughes, G. Poudel, J. F. Domínguez, and K. Caeyenberghs. 2020. "Structure-function relationships in brain-injured patients: a scoping review."
Paus, T., Paseresi, M., French, L., 2014. White matter as a transport system. Neuroscience 276, 117–125.
Pfefferbaum, A., Chanraud, S, Pitel, A.L, Müller-Oehring, E., Shankaranarayanan, A, Alsop, D.C., Rohlfing, T., Sullivan, E.D., 2010. Cerebral blood flow in posterior cortical nodes of the default mode network decreases with task engagement but remains higher than in most brain regions. Cereb. Cortex 21, 233–244.
Raichle, M.E., Macleod, A.M., Snyder, A.Z., Powers, W., Gusnard, D.A., Shulman, G., 2001. A default mode of brain function. Proc. Natl. Acad. Sci. United States America 98 (2), 676–682.
Rosen, Burke Q, Halgren, Eric, 2022. An estimation of the absolute number of axons indicates that human cortical areas are sparsely connected. PLoS Biol. 20 (3), e3001575.
Royer, J., Rodríguez-Cruces, R., Tavakol, S., et al., 2022. An open MRI dataset for multiscale neuroscience. Sci Data 9, 569. doi:10.1038/s41597-022-01682-y.
Rushton, W.A.H., 1951. A theory of the effects of fibre size in medullated nerve. J. Physiol. 115, 101–122.
Ryali, S., Chen, T., Supekar, K.K., Menon, V., 2012. Estimation of functional connectivity in fMRI data using stability selection-based sparse partial correlation with elastic net penalty. Neuroimage 59 (4), 3852–3861.
Sanchez-Romero, Ruben, Cole, Michael W., 2020. Combining multiple functional connectivity methods to improve causal inferences. J. Cogn. Neurosci. 33 (2), 180–194.
Sarwar, T., Tian, Y., Yeo, B.T.T., Ramamohanarao, K., Zalesky, A., 2021. Structure-function coupling in the human connectome: a machine learning approach. Neuroimage 226 (1), 117609 11 pages.
Schaefer, Alexander, Kong, Ru, Gordon, Evan M, Laumann, Timothy O, Zuo, Xi-Nian, Holmes, Avram J, Eickhoff, Simon B, Thomas Yeo, B T, 2018. Local-global parcellation of the human cerebral cortex from intrinsic functional connectivity MRI. Cereb. Cortex 28 (9), 3095–3114.
Schirner, Michael, McIntosh, Anthony Randal, Jirsa, Viktor, Deco, Gustavo, Ritter, Petra, 2018. Inferring multi-scale neural mechanisms with brain network modelling. Elife 7 January.
Schrijver, Alexander., 2002. On the history of the transportation and maximum flow problems. Math. Program. 91 (3), 437–445.
Seeley, W.W., 2019. The salience network: a neural system for perceiving and responding to homeostatic demands. J. Neurosci. 39 (50), 9878–9882.
Seeley, W.W., Menon, V., Schatzberg, A.F., Keller, J., Glover, G.H, Kenna, H., Reiss, A.L., Grecius, M.D., 2007. Dissociable intrinsic connectivity networks for salience processing and executive control. J. Neurosci. 27 (9), 2349–2356.
Seguin, C., van den Heuvel, M.P., Zalesky, A., 2018. Navigation of brain networks. Proc. Natl. Acad. Sci. United States America 115 (24), 6297–6302.
Simoncelli, Eero P, Olshausen, Bruno A, 2001. Natural image statistics and neural representation. Annu. Rev. Neurosci. 24 (1), 1193–1216. doi:10.1146/annurev.neuro.24.1.1193.
Smith, R., Raffelt, D., Tournier, J., & Connelly, A. (2020, July 20). Quantitative streamlines tractography: methods and inter-subject normalisation. doi:10.31219/osf.io/c67kn.
Smith, R., Tournier, J.D., Calamante, F., Connelly, A., 2015. SIFT2: enabling dense quantitative assessment of brain white matter connectivity using streamlines tractography. Neuroimage 1 (119), 35–51.
Smith, S., Vidaurre, D., Beckmann, C.F., Glasser, M.F., Jenkinson, M., Miller, K.L., Nichols, T.E., et al., 2013. Functional connectomics from resting-state fMRI. Trends Cogn. Sci. 17 (12), 666–682.
Spead, Olivia, Poulain, Fabienne E, 2020. Trans-axonal signaling in neural circuit wiring. Int. J. Mol. Sci. 21 (14), 5170.
Sporns, O., 2013. Structure and function of complex brain networks. Dialogues Clin. Neurosci. 15 (3), 247–262.
Spruston, Nelson, Häusser, Michael, Stuart, Greg, 2013. Information processing in dendrites and spines. In: Fundamental Neuroscience. Elsevier, pp. 231–260. doi:10.1016/b978-0-12-385870-2.00011-1.
Straathof, M., Sinke, M., Dijkhuizen, R., Otte, W., 2018. A systematic review on the quantitative relationship between structural and functional network connectivity strength in mammalian brains. J. Cereb. Blood Flow Metab. 39 (2), 189–209.
Suárez, L., Markello, R., Betzel, R., Misic, B., 2020. Linking structure and function in macroscale brain networks. Trends Cogn. Sci. 24 (4), 302–315.
Supekar, K., Uddin, L.Q., Prater, K., Amin, H., Greicius, M.D., Menon, V., 2010. Development of functional and structural connectivity within the default mode network in young children. Neuroimage 52 (1), 290–301.
Tewarie, P., Hillebrand, A., van Dijk, B.W., Stam, C.J., OŃeill, G.C., Van Mieghem, P., Meier, J.M., Woolrich, M.W., Morris, P.G., Brookes, M.J., 2016. Integrating cross-frequency and within band functional networks in resting-state MEG: a multi-layer network approach. Neuroimage 142, 324–336.
Tiepel, S., Bodke, A., Meindl, T., Amaro, E., Soldner, J., Reiser, M., Herpertz, S.C., Möller, Hans-Jürgen, Hampel, Harald, 2010. White matter microstructure underlying default mode network connectivity in the human brain. Neuroimage 49 (3), 2021–2032. doi:10.1016/j.neuroimage.2009.10.067.
Uddin, N., Figley, T.D., Solar, K.G., Shatil, A.S., Figley, C.R., 2019. Comparisons between multi-component myelin water fraction, T1w/T2w ratio, and diffusion tensor imaging measures in healthy human brain structures. Sci. Rep. 9, 3013.
Vàzquez-Rodríguez, B., Suárez, L.E., Markello, R.D., Shafiei, G., Paquola, C., Hagmann, P., van den P Heuvel, M.P., Bernhardt, B.C., 2019. Gradients of structure–function tethering across neocortex. PLoS Biol. 116 (42), 21219–21227.
Wang, Yanjiang, Chen, Xue, Liu, Baodi, Liu, Weifeng, Shiffrin, Richard M, 2020. Understanding the relationship between human brain structure and function by predicting the structural connectivity from functional connectivity. IEEE Access 8, 209926–209938.
Watts, D J, Strogatz, S H, 1998. Collective dynamics of 'small-world' networks. Nature 393 (6684), 440–442.
Yeh, F.C., Verstynen, T.D., Wang, Y., Fernández-Miranda, J.C., Tseng, W.Y.I., 2013. Deterministic diffusion fiber tracking improved. PLOS 8, E80713.
Yeh, Fang-Cheng., 2020. Shape analysis of the human association pathways. Neuroimage 223 (117329), 117329.
Yeh, F., Wedeen, V., Tseng, W., 2010. Generalized q-sampling imaging. IEEE Trans. Med. Imaging 29, 1626–1635.
Yeo, B T Thomas, Krienen, Fenna M, Sepulcre, Jorge, Sabuncu, Mert R, Lashkari, Danial, Hollinshead, Marisa, Roffman, Joshua L, et al., 2011. The organization of the human cerebral cortex estimated by intrinsic functional connectivity. J. Neurophysiol. 106 (3), 1125–1165.
Zalesky, A., Fornito, A., Cocchi, L., Gollo, L.L., van den Heuvel, M.P., Breakspear, M., 2016. Connectome sensitivity or specificity: which is more important? Neuroimage 142, 407–420.
Zalesky, A., Fornito, A., Harding, I.H, Cocchi, L., Yücel, M., Pantelis snd E. T. Bullmore, C., 2010. Whole-brain anatomical networks: does the choice of nodes matter? Neuroimage 50, 970–983.
Zhan, Liang, Jenkins, Lisanne M., Wolfson, Ouri E., GadElkarim, Jounson Jonaris, Nocito, Kevin, Thompson, Paul M, Ajilore, Olusola A, Chung, Moo K, Leow, Alex D, 2017. The significance of negative correlations in brain connectivity. J. Computat. Neurol. 15 (15), 3251–3265.
Zikopoulos, B, Barbas, H, 2010. Changes in prefrontal axons may disrupt the network in autism. J. Neurosci. 30 (44), 14595–14609.
Zou, Hui, Hastie, Trevor, 2005. Regularization and variable selection via the elastic net. J. R. Stat. Soc. Ser. B Stat. Methodol. 67 (2), 301–320.